Articles

Catalysis and Function of the p38α·MK2a Signaling Complex

Susan M. Lukas,‡ Rachel R. Kroe,‡ Jessi Wildeson, Gregory W. Peet, Lee Frego, Walter Davidson, Richard H. Ingraham, Christopher A. Pargellis, Mark E. Labadia,* and Brian G. Werneburg*

Department of Immunology and Inflammation, Research and Development Center, Boehringer Ingelheim Pharmaceuticals, 900 Ridgebury Road, Ridgefield, Connecticut 06877

Received March 11, 2004; Revised Manuscript Received May 30, 2004

ABSTRACT: The p38 mitogen-activated protein kinase (p38) pathway is required for the production of proinflammatory cytokines (TNFα and IL-1) that mediate the chronic inflammatory phases of several autoimmune diseases. Potent p38 inhibitors, such as the slow tight-binding inhibitor BIRB 796, have recently been reported to block the production of TNFα and IL-1β. Here we analyze downstream signaling complexes and molecular mechanisms, to provide new insight into the function of p38 signaling complexes and the development of novel inhibitors of the p38 pathway. Catalysis, signaling functions, and molecular interactions involving p38α and one of its downstream signaling partners, mitogen-activated protein kinase-activated protein kinase 2 (MK2), have been explored by steady-state kinetics, surface plasmon resonance, isothermal calorimetry, and stopped-flow fluorescence. Functional 1/1 signaling complexes ($K_d = 1-100$ nM) composed of activated and nonactivated forms of p38α and a splice variant of MK2 (MK2a) were characterized. Catalysis of MK2a phosphorylation and activation by p38α was observed to be efficient under conditions where substrate is saturating ($k_{cat}^{app} = 0.05-0.3\ s^{-1}$) and nonsaturating ($k_{cat}^{app}/K_M^{app} = 1-3 \times 10^6\ M^{-1}\ s^{-1}$). Specific interactions between the carboxy-terminal residues of MK2a (370−400) and p38α precipitate formation of a high-affinity complex ($K_d = 20$ nM); the p38α-dependent MK2a phosphorylation reaction was inhibited by the 30-amino acid docking domain peptide of MK2a ($IC_{50} = 60$ nM). The results indicate that the 30-amino acid docking domain peptide of MK2a is required for the formation of a tight, functional p38α·MK2a complex, and that perturbation of the tight-docking interaction between these signaling partners prevents the phosphorylation of MK2a. The thermodynamic and steady-state kinetic characterization of the p38α·MK2a signaling complex has led to a clear understanding of complex formation, catalysis, and function on the molecular level.

Induced by stress and inflammation, the p38[1] pathway is a complex cascade of protein kinases that mediate multiple cellular functions, including migration (*1*, *2*), death (*3*), survival (*4*), and proinflammatory cytokine production (*5*). A family of p38 kinases at the center of the pathway is composed of α, β, γ, and δ isoforms; this family of enzymes modulates the functions of numerous downstream effector proteins. Recent p38α isoform genetic deletion studies and p38α inhibition studies have implied that this isoform plays an important role in signaling the production of inflammatory cytokines. Embryonic stem cells derived from mice that lack p38α exhibit impaired IL-1 signaling (*6*). Reversible inhibition of p38α (and also p38β) by the classical p38 inhibitor, SB203580 (*7*), and more potent compounds, such as BIRB 796 (*8*, *9*), inhibits the lipopolysaccharide-induced production of proinflammatory cytokines, including TNFα and IL-1, that are implicated in the etiology of chronic inflammation (*10*−*13*). Therefore, p38α is a prime target for the development of anti-inflammatory drugs.

p38α transduces signals through downstream effectors, including transcription factors, elongation factors, and MKs. Genetic deletion and phosphorylation studies indicate that MK2 also participates in modulating the production of inflammatory cytokines; thus, it too is a primary target for the abatement of chronic inflammation. Discovered in 1992 (*14*, *15*), MK2 was first observed to be activated by ERK *in vitro*, and shortly thereafter to be activated by p38 in cells

* To whom correspondence should be addressed. Telephone: (203) 798-5518. Fax: (203) 791-6196. E-mail: bwernebu@rdg.boehringer-ingelheim.com and mlabadia@rdg.boehringer-ingelheim.com.

‡ These authors contributed equally to this work.

[1] Abbreviations: ATF-2, activating transcription factor 2; CHAPS, 3-[(3-cholamidopropyl)dimethylammonio]-1-propanesulfonate; DTT, dithiothreitol; EDTA, ethylenediaminetetraacetic acid; EGTA, (ethylenedioxy)diethylenedinitrilotetraacetic acid; ESI, electrospray ionization; FITC, fluorescein isothiocyanate; GSH, glutathione; GST, glutathione *S*-transferase; HEPES, 4-(2-hydroxyethyl)-1-piperazineethanesulfonic acid; His, histidine; HSP27, heat shock protein 27; IFNγ, interferon γ; IL, interleukin; ITC, isothermal titration calorimetry; LSP1, lymphocyte specific protein 1; MK, mitogen-activated protein kinase-activated protein kinase; MEF, myocyte enhancing factor; μLC−FTMS, micro high-performance liquid chromatography−Fourier transform mass spectrometry; p38, p38 mitogen-activated protein kinase; PMSF, phenylmethanesulfonyl fluoride; SPR, surface plasmon resonance; SRF, serum response factor; TCEP, tris(2-carboxyethyl)phosphine hydrochloride; TES, *N*-tris(hydroxymethyl)methyl-2-aminoethanesulfonic acid; TEV, tobacco etch virus; TNFα, tumor necrosis factor α.

10.1021/bi049508v CCC: $27.50
Published on Web 07/16/2004

(*16*−*18*). Experiments with mice genetically deficient in MK2 confirm that the enzyme is involved in transmitting p38 pathway-dependent signals required for cytokine production. $MK2^{-/-}$ mice challenged with lipopolysaccharide produce significantly less TNFα, IL-1, IL-6, and IFNγ than wild-type mice stimulated with a lipopolysaccharide (*19*). In addition, $MK2^{-/-}$ mice brains produce less IL-1β in response to ischemia than $MK2^{+/+}$ mouse brains, and they display a reduction in infarct size and protection of neuronal function (*3*). The mechanisms by which MK2 regulates the production of inflammatory cytokines are not yet completely understood, but they appear to involve the AU-rich elements at the 3′-untranslated regions of cytokine mRNA, and MK2 phosphorylation of factors that bind to the AU-rich elements. AU-rich element modulation of cytokine message stability and translation is at least partly mediated by MK2-dependent processes (*19*−*22*).

There are two known splice variants of MK2. The first variant, MK2a (*14*, *15*), contains a nuclear localization sequence bound by residues 373−389 (*23*, *24*) and a putative docking domain for p38 located near the carboxy terminus. This domain is thought to interact with two acidic regions of p38α known as the CD domain, residues D313−D316 (*25*), and the ED domain, residues E160 and D161 (*26*). The interactions between p38α and homologues of MK2, MK3, and MK5 (also known as PRAK) have been shown to be dependent on the CD and ED domains by mutagenesis studies and pull-down (interaction) assays (*26*). Pull-down assays with MK2a and p38α indicate that the 377−400-amino acid carboxy-terminal domain of MK2a does interact with p38α (*27*). The interaction between MK2a and p38α has not yet been characterized in thermodynamic or structural studies; however, non-steady-state kinetics experiments indicate that p38α is a good catalyst of MK2a phosphorylation. The apparent second-order rate constant (k_{cat}/K_M) for phosphorylation of MK2a by p38α is 34 000 M^{-1} s^{-1} (*28*). Immunocomplex kinase assays and overexpression studies also indicate that MK2a is phosphorylated by the α and β isoforms of p38, but not the δ and γ isoforms (*29*, *30*). A second splice variant of MK2, MK2b (*31*, *32*), contains an identical amino-terminal kinase domain, but lacks a nuclear localization sequence and a p38 docking domain (*23*, *24*). MK2b is also phosphorylated by p38α, but the catalytic efficiency of phosphorylation and the binding affinity of MK2b for p38α have not been well characterized.

At least four residues of MK2a (also found in MK2b) are phosphorylated by p38α: T25, T222, S272, and T334 (*33*). Phosphorylation of three of these residues (T222, S272, and T334) has been reported to be required for maximal activation of MK2a (*33*), and the phosphorylation of T334 is reported to expose a nuclear export sequence that leads to the nucleocytoplasmic transport of MK2a and p38 (*23*, *24*, *34*). The activation of the MK2 splice variants under steady-state conditions has not yet been studied, and the relative rates of phosphorylation at individual MK2 residues have not been well characterized.

A clearer understanding of p38α signaling complexes and functions on the molecular level is a prerequisite for the development of novel inhibitors designed to specifically block the production of proinflammatory cytokines downstream of p38α. Quantitative analyses of the formation of complexes composed of p38α and the MK2 splice variants would greatly improve our understanding of the functions of these complexes. A steady-state kinetic study of MK2 splice variant phosphorylation and activation by p38α would also add to our understanding of the catalysis of activation of these signaling complexes.

We have employed steady-state kinetics, surface plasmon resonance, isothermal titration calorimetry, and stopped-flow fluorescence spectroscopy to characterize the p38α·MK2 signaling complexes kinetically and thermodynamically. These kinetic and thermodynamic studies have led to the discovery of high-affinity p38α·MK2a complexes that provide new insight into p38α·MK2a complex formation, function, and catalysis. A novel mechanism of p38α pathway inhibition, perturbation of the docking interaction between p38α and MK2a substrate, is also described.

EXPERIMENTAL PROCEDURES

Expression and Purification of Signaling Reagents. The cDNA encoding murine p38α was cloned into pET15b (Novagen), expressed in *Escherichia coli* with a five-His affinity tag at the amino terminus, and purified to greater than 95% purity, as described previously (*35*). The enzyme was activated by dual phosphorylation of the TGY sequence (74% as determined by mass spectrometry) with the activated MKK3 kinase domain in a reaction mixture containing 200 nM activated MKK3 kinase domain, 15 μM p38α, and 1 mM ATP. The reaction buffer consisted of 50 mM HEPES (pH 7.6), 50 mM KCl, 15 mM $MgCl_2$, 100 μM Na_3VO_4, 0.01% CHAPS, 1 mM DTT, and 10 μg/mL bovine serum albumin. The phosphatase inhibitor, Na_3VO_4, was added as a precautionary measure. The reaction was halted after incubation for 6 h at 25 °C and incubation for 12 h at 4 °C by desalting on a 10 mL Econo-Pac 10 DG desalting column (Bio-Rad) equilibrated in 20 mM HEPES (pH 7.6), 500 μM EDTA, 100 mM NaCl, 10% glycerol, and 1 mM DTT. Activated p38α was stored at −80 °C.

The cDNA encoding human GST-MK2a 1−400, which contains the p38 docking domain, nuclear localization sequence, and nuclear export sequence at the carboxy terminus (*14*, *15*, *23*, *24*), was cloned into pVL1393 (Invitrogen) and expressed in SF21 cells by standard procedures. The MK2a clone was created from the MK2b splice variant DNA (*31*, *32*) with one mutation at the amino terminus, L2V. The MK2b clone was used as a template in four consecutive PCRs to generate MK2a 1−400. The forward primer in the first three PCRs was 5′-ATCAAACTTGGATCCCATGGTGTCCAACTCCCAGG. Three reverse primers were used in three consecutive reactions: 1, 5′-GTAGTCTACTCTCATTGTGGCCAGTGCGGATGTCATTTCTTCCTTGACATCCTCCCACCGCTCC; 2, 5′-CGGGTTGGAGGCGTCTTCGATTTTTTTGATTTTGATCTGTTCGTAGTCTACTCTCATTGTGGCC; and 3, 5′-CTGCTTCCAGTGCGCGTGCTTTTTTGCGGCGTTTCAGCAGCAGCGGGTTGGAGGCGTCTTCG. The final reaction was performed with a distinct forward primer (5′-GGATCCATGGTGTCCAACTCCCAG) and the fourth reverse primer (5′-AGTCACGATGCGGCCGCTTACTAGTGTGCCAGTGCTGCTGCTTCCAGTGCGCGTGC). The gene was then inserted downstream of GST and a TEV cleavage site in pVL1393 utilizing *Bam*HI and *Not*I restric-

tion sites. TEV cleavage of the fusion protein produced full-length MK2a 1−400 with one additional serine residue at the amino terminus. Insect cells expressing the GST fusion protein were lysed by dounce homogenization in 20 mM HEPES (pH 7.6), 10 mM sodium bisulfite, 1 mM DTT, 0.02 mg/mL pepstatin A, 0.02 mg/mL leupeptin, and 0.1 mM PMSF. The cell lysates were clarified by centrifugation at 44 000 rpm for 1 h.

A deletion mutant of the MK2 splice variant that lacks the carboxy-terminal nuclear localization sequence, GST−MK2b 41−370 (*31*, *32*), was cloned into pGEX-4T and expressed in *E. coli* BL21(DE3) pLysS. The first 40 amino acids of MK2b, rich in glycine and proline codons, were removed to improve the protein expression efficiency in *E. coli*. The cDNA encoding GST−ATF-2 1−109 and additional residues at the carboxy terminus, GEFIVTD, was cloned into pGEX-2T and expressed in *E. coli* BL21(DE3) pLysS. The cDNA encoding GST−LSP1 179−339 was cloned into pGEX-4T and expressed in *E. coli* BL21(DE3) pLysS. The expression hosts were grown in 2XTY medium, containing 50 μg/mL ampicillin and 34 μg/mL chloramphenicol, at 37 °C to an optical density of 0.5 at 600 nm. The cultures were induced with 0.1 mM IPTG at 25 °C, and after induction for 7 h, the cells were harvested by centrifugation. The cells were lysed by sonication with a Branson 450 sonifier in 20 mM HEPES (pH 7.6), 10% glycerol, 0.2 M NaCl, 1 mM EDTA, 1 mM EGTA, 1 mM DTT, and 0.1 mM PMSF. The cell lysates were clarified by centrifugation.

The GST fusion proteins were purified by affinity chromatography using GSH-Trap (Amgen) affinity chromatography columns or GSTPREP FF 16/10 (Amgen) columns to >95% purity. The clarified lysates were loaded on the affinity columns equilibrated in 20 mM HEPES (pH 7.6), 10% glycerol, 1 mM EDTA, 1 mM EGTA, 1 mM DTT, 0.1 mM PMSF, and 150 mM NaCl. The columns were washed in the same buffer containing 400 mM NaCl. The GST fusion proteins were eluted with 20 mM HEPES (pH 7.6), 10% glycerol, 1 mM EDTA, 1 mM EGTA, 1 mM DTT, 0.1 mM PMSF, 150 mM NaCl, and 10 mM glutathione. The purified proteins were dialyzed against 20 mM HEPES (pH 7.6), 10% glycerol, 1 mM EDTA, 1 mM EGTA, 1 mM DTT, and 300−400 mM NaCl to remove glutathione. The purified proteins were stored at −80 °C.

Deletion mutants of MK2a that contain a six-His amino-terminal fusion, 6His-MK2a 51−369 and 6His-MK2a 51−400, were cloned into pET23a (Novagen) and expressed in *E. coli* as described above. The histidine-tagged proteins were lysed in 20 mM HEPES (pH 8), 300 mM NaCl, 10% glycerol, and EDTA-free protease inhibitor tablets (Roche). A polytron homogenizer was used at speed 15 for 2 min, followed by sonication with a Branson 450 sonifier. The cell lysates were clarified by centrifugation as described above. Each clarified lysate was loaded onto a Ni−NTA Superflow (Qiagen) column equilibrated in 20 mM HEPES (pH 7), 50 mM NaCl, 10% glycerol, and 10 mM imidazole. The protein was eluted in the same buffer containing 250 mM imidazole; 2 mM DTT and 2 mM EDTA were added to the eluted protein fraction, and the protein fraction was diluted by a factor of 1.5 by the addition of HEPES (pH 7), 50 mM NaCl, and 10% glycerol. The proteins were further purified by cation exchange chromatography on S 25 μm (Bio-Rad) resin with a 50 mM to 1 M NaCl gradient in 20 mM HEPES (pH 7), 50 mM NaCl, 10% glycerol, and 1 mM DTT. The purified proteins were stored at −80 °C.

MK2a 370−400 (IKIKKIEDASNPLLLKRRKKARALE-AAALAH) and FITC−MK2a 370−400 peptides were synthesized and purified by Anaspec.

*Activation of p38*α. Purified p38α was activated by dual phosphorylation of the TGY sequence (74% as determined by mass spectrometry) in a reaction catalyzed by active MKK3a 6−315. p38α (15 μM) was incubated with active MKK3a 6−315 (200 nM) and 1 mM ATP for 6 h at 25 °C in 50 mM HEPES (pH 7.6), 50 mM KCl, 15 mM $MgCl_2$, 100 μM Na_3VO_4, 0.01% CHAPS, 1 mM DTT, and 10 μg/mL bovine serum albumin. Activated p38α was desalted on a 10 mL Econo-Pac 10 DG desalting column (Bio-Rad) equilibrated in 20 mM HEPES (pH 7.6), 500 μM EDTA, 100 mM NaCl, 10% glycerol, and 1 mM DTT.

Steady-State Kinetics Assays. The phosphorylation of MK2a and MK2b catalyzed by active murine p38α was assessed at 25 °C in 50 mM HEPES (pH 7.6), 50 mM KCl, 10 mM $MgCl_2$, 100 μM Na_3VO_4, 0.01% CHAPS, 1 mM DTT, 10 μg/mL bovine serum albumin, and [γ-^{33}P]ATP (500−2000 Ci/mol). The specific details pertaining to enzyme assays are provided in the figure legends. Briefly, the phosphorylation of MK2 constructs by catalytic amounts of active p38 isoforms was quenched with 10% trichloroacetic acid and 5% inorganic pyrophosphate. Phosphorylated MK2 products were captured with filter plates followed by scintillation counting to determine the moles of product formed. The velocity of product formation was determined by linear regression, and Michaelis−Menten constants were obtained from hyperbolic curve fits to the Michaelis−Menten equation [$v = V_{max}[S]/(K_M + [S])$]. The observed rate constants for phosphorylation of GST−LSP1 179−339 (10 μM) by active MK2a (1 nM) were measured in the same reaction buffer containing 150 μM [γ-^{33}P]ATP (800 Ci/mol). The initial velocity of phosphorylation was measured by quenching and scintillation counting, as described for p38 catalysis.

MK2a Phosphorylation Analysis by Mass Spectrometry. 6His-MK2a 51−400 (11.5 μM) was phosphorylated with 95 nM active p38α in 50 mM HEPES (pH 7.6), 1 mM ATP, 50 mM KCl, 25 mM $MgCl_2$, 100 μM Na_3VO_4, 0.01% CHAPS, 1 mM DTT, and 5 mM NaF. The phosphatase inhibitors, Na_3VO_4 and NaF, were added to the reaction buffer as a precautionary measure against phosphatase activity. Samples (500 μL) were quenched at various times with 100 mM EDTA, and desalted on 10 mL Econo-Pac 10 DG desalting columns from Bio-Rad equilibrated in 20 mM HEPES (pH 7.6), 500 μM EDTA, 100 mM NaCl, 10% glycerol, 1 mM DTT, 100 μM PMSF, 100 μM Na_3VO_4, and 5 mM NaF. A 25 μL aliquot of each sample was added to 25 μL of 0.4 M NH_4HCO_3 in 4 M urea and 5 μL of 45 mM DTT. This solution was incubated at 50 °C for 15 min and then cooled to room temperature. A 5 μL aliquot of 100 mM iodoacetamide was added, and the solution was incubated at room temperature for 15 min. H_2O (40 μL) and trypsin (5 μL of a 0.4 mg/mL solution) were added to digest the samples at 37 °C overnight.

A 10 μL aliquot of each digest was injected onto a PepMap (LC Packings, San Francisco, CA) C18 column (1.0 mm × 15 cm). A gradient elution from 0% to 60% B in 55 min, at a flow rate of 40 μL/min, with mobile phase A (99/1/0.1

H_2O/acetonitrile/formic acid mixture) and mobile phase B (10/90/0.1 H_2O/acetonitrile/formic acid mixture) was used. Selected ion monitoring was performed at *m*/*z* 568.4, 608.4, 866.2, 886.2, 970.8, and 990.8 with an Ultima MS (Micromass, Manchester, U.K.). The dwell time was 0.5 s, the cone voltage 50 V, the interchannel delay time 0.1 s, and the interscan delay time 0.1 s. The peak heights were used for calculations. The fraction phosphorylated was determined as the response for the phosphorylated peptide divided by the response for phosphorylated and unphosphorylated for each peptide monitored within each run.

A separate μLC/FTMS experiment was performed to identify tryptic cleavage sites and confirm assignment of the monitored peptides within *m*/*z* ±5 ppm of theoretical. A 20 μL aliquot was injected onto a 150 mm × 0.3 mm PepMap C18 column, and the sample was eluted with a complex water/acetonitrile/formic acid gradient over 54 min at 4 μL/min. The eluent was monitored, after a 700 s delay, by ESI FTMS with a Bruker APEX II instrument (Bruker, Billerica, MA). Data were acquired for *m*/*z* 400−1600, 256 K word, averaging seven 1 s acquisitions into each of 128 spectra. Spectra were converted to Masslynx format (Micromass) for analysis.

p38α Inhibition. The inhibition of activated p38α catalysis of ATF-2 phosphorylation was assessed directly as described above with [γ-^{33}P]ATP, and filter plates were used to capture phosphorylated ATF-2. However, the inhibition of MK2a phosphorylation and activation was assessed indirectly through a substrate of MK2a, GST−LSP1 179−339. This was necessary to facilitate the assessment of competition between inhibitors and MK2a for p38α. The inhibition of MK2a activation was assessed in the presence of 250 pM p38α, 25 nM 6His-MK2a 51−400, and 10 μM GST−LSP1 179−339. GST−LSP1 179−339 phosphorylated by MK2a was precipitated with 10% trichloroacetic acid and 5% inorganic pyrophosphate, and captured with filter plates as described previously.

Analytical Ultracentrifugation. Experiments were performed using a Beckman model XL-I analytical ultracentrifuge. Predicted partial specific volumes, extinction coefficients, and solvent densities were calculated using SEDNTERP (available at http://www.bbri.org/rasmb/rasmb.html) for use in data analysis. The predicted partial specific volumes used in these analyses for p38α and MK2a are 0.7369 and 0.7391 mL/g, respectively. All data were fit using a solvent density of 1.00704 g/mL.

Sedimentation velocity experiments were conducted for p38α (4.5 μM) and MK2a (12.6 μM) in 20 mM TES (pH 7.0), 200 mM NaCl, 0.05% CHAPS, and either 1 mM TCEP or 0.5 mM DTT at 20 °C using double sector centerpieces and quartz windows. Data were collected at 50 000 rpm and either 240 or 280 nm. Data were analyzed using Sedfit version 8.4 (available at http://analyticalultracentrifugation.com/).

Sedimentation equilibrium experiments were conducted for p38α and MK2a in 20 mM TES (pH 7.0), 200 mM NaCl, and 1 mM TCEP at 20 °C using six-channel centerpieces and quartz windows. Data were collected at 280 nm for multiple concentrations and multiple rotor speeds (8000, 12 000, 16 000, and 20 000 rpm). Data were analyzed using WinNonlin version 1.08 (available at http://www.bbri.org/rasmb/rasmb.html).

Surface Plasmon Resonance. All SPR experiments were performed on a BIAcore 3000 instrument (BIAcore, Inc.). Anti-GST antibody (BIAcore, Inc.), 20 μg/mL, in 10 mM sodium acetate (pH 5.0) was immobilized to 3000 resonance units on a BIAcore CM4 chip using a standard amine-coupling protocol (*36*). GST−MK2a 1−400 was injected over the anti-GST surface at 500 nM in the following buffer: 50 mM Tris-HCl (pH 8.0), 100 mM NaCl, 0.01% BSA, 0.01% CHAPS, and 500 μM TCEP. GST−MK2a 1−400 was injected over the anti-GST surface until a density of 300−400 resonance units was reached.

Determination of Binding Constants for p38α by SPR. All equilibrium experiments were carried out at 25 °C in the buffer mentioned above, containing 100 or 350 mM NaCl. Equilibrium binding data for binding of p38α to immobilized MK2a were obtained by titrating phosphorylated and non-phosphorylated p38α over the GST−MK2a 1−400 surface at a flow rate of 30 μL/min. Equilibrium data were collected, and the K_d for the p38α·MK2a interaction was estimated by nonlinear regression analysis using the Marquardt−Levenburg minimization method (*37*).

Isothermal Titration Calorimetry. The isothermal titration calorimetry experiments were performed using a Microcal VP-ITC instrument (Microcal, Inc., Northampton, MA). The sample cell of the calorimeter was loaded with MK2a (5−22 μM) in 20 mM TES (pH 7.0), 200 mM NaCl, and 1 mM TCEP. The syringe was loaded with murine p38α (37−167 μM) in the same buffer. All solutions were degassed for 8 min. Titrations were performed at 25 °C with injection volumes ranging from 4 to 12 μL and a spacing of 500 s. After completion of the titration, baselines were manually drawn and subtracted from the data. The baseline was set to zero assuming that the final injections of each titration represent only the heat of dilution. The data were fit using a one-site binding model available in the Origin ITC data analysis software (version 5.0).

Stopped-Flow Fluorescence. All kinetic constants were determined using a KinTek (Austin, TX) stopped-flow instrument, model SF-2001. The assay buffer for all experiments consisted of 20 mM TES (pH 7.0) and 200 mM NaCl. Kinetic binding reactions were initiated at a flow rate of 15 mL/s, and the sample was excited in an 80 μL quartz observation cell at 494 nm through a Glan-Thompson polarizer, employing a 75 W xenon arc lamp. The relative emission intensities of the parallel and perpendicular components were measured in the T-format through two photomultiplier tubes with attached film polarizers and 530 nm long wave pass filters. Data acquisition began at the start of the injection with a dead time of approximately 0.002 s, and continued until the reaction had reached equilibrium. The reaction temperature was held at 22 °C using an external water bath.

Rate Constants for Binding of the FITC−MK2a 370−400 Peptide to p38α. The association constant (k_{on}) and dissociation constant (k_{off}), describing the interaction between the FITC−MK2a 370−400 peptide and p38α, were determined by performing the kinetic assay as two half-reactions. The first half-reaction, monitoring the association kinetics of the p38α·FITC−MK2a 370−400 peptide complex, consisted of loading FITC−MK2a 370−400 peptide (250 nM) in one of the stopped-flow syringes and p38α (400 nM) in the other syringe. The second half-reaction, monitoring the dissociation

kinetics, consisted of preincubating the p38α·FITC−MK2a 370−400 peptide complex in one syringe and loading excess unlabeled MK2a 370−400 peptide in the other syringe (2 μM). At such high concentrations, reassociation of the FITC−MK2a 370−400 peptide is negligible. The complementary data from the two half-reactions in the direct binding assay can be combined into a single data set and modeled simultaneously to fit for the rate constants. The derivation of the integrated rate equation describing the overall kinetic binding reaction has been described previously (*38*). All of the data were analyzed using the SAS 8.0 statistical software system. Parameter estimates (k_{on} and k_{off}) were obtained by applying ordinary nonlinear least-squares regression techniques to a kinetic model (*38*) using the Marquardt−Levenberg minimization method. The k_{on} and k_{off} determined here for the p38α·FITC−MK2a 370−400 peptide complex were employed in the ligand exchange assay described below to evaluate the kinetics of binding of various unlabeled MK2a constructs.

Ligand-Exchange Binding Assay. Paired ligand-exchange assays were performed to determine the kinetic rate constants for the binding of various unlabeled MK2a constructs, including 6His−MK2a 51−400, to p38α. The experimental conditions and instrumentation employed in this assay are the same as described above for the direct binding assay. The association rate for the unlabeled MK2a construct was determined by preincubating p38α with the FITC−MK2a 370−400 peptide, followed by rapid mixing with the unlabeled MK2a construct. The change in fluorescence anisotropy due to the displacement of the FITC−MK2a 370−400 peptide was monitored. The dissociation rate of the unlabeled MK2a construct was measured by preincubating p38α with the unlabeled MK2a construct, followed by mixing with the FITC−MK2a 370−400 peptide. The data from the paired ligand-exchange assays were combined and analyzed, as described above in the direct binding assay section.

RESULTS

Biophysical Characterization of the p38α·MK2a Complex. The p38 pathway components utilized in the following kinetic and thermodynamic studies were purified to homogeneity and characterized by sedimentation velocity and sedimentation equilibrium. Sedimentation velocity experiments with p38α and 6His−MK2a 51−400 indicated that both proteins are monomeric with $S_{20,w}$ values of 3.28 and 3.0, respectively. A small amount of aggregate, typically less than 5%, was present in both the p38α and 6His−MK2a 51−400 preparations. This aggregate can be removed by size-exclusion chromatography and is not in reversible equilibrium with the monomeric species (data not shown). To account for the small amount of aggregate present in the samples, sedimentation equilibrium data were fit allowing for the presence of a small amount of dimer. The apparent solution molecular masses for p38α and MK2a were calculated to be 39.5 (38.1, 40.9) kDa and 39.6 (36.8, 42.9) kDa, respectively. These values are consistent with the monomer molecular masses of 41.9 kDa for p38α and 41.2 kDa for 6His−MK2a 51−400 predicted from the amino acid sequences. Predicted sequence molecular masses were confirmed by mass spectrometry (data not shown).

Table 1: Surface Plasmon Resonance Analysis of p38α·MK2a Complexes

immobilized sample	titrant	[NaCl] (M)	K_d (nM)	n
GST−MK2a 1−400	p38α	0.1	2.5 ± 0.5	3
GST−MK2a 1−400	p38α	0.35	65 ± 7	4
GST−MK2a 1−400	activated p38α	0.1	6.3 ± 2.4	3
GST−MK2a 1−400	activated p38α	0.35	122 ± 25	4
activated GST−MK2a 1−400	p38α	0.1	104 ± 30	3
activated GST−MK2a 1−400	activated p38α	0.1	60.0 ± 3.5	3
GST−MK2b 41−370	p38α	0.1	>5000	1

Table 2: Stopped-Flow Fluorescence Analysis of p38α·MK2a Complexes

reactants	k_{on} (M^{-1} s^{-1})	k_{off} (s^{-1})	K_d (nM)
p38α, FITC−MK2a 370−400	(1.9 ± 0.5) × 10^8	1.6 ± 0.1	8.4
p38α, MK2a 370−400	(4.2 ± 1.4) × 10^8	8.4 ± 2.3	20
p38α, 6His−MK2a 51−400	(6.6 ± 1.9) × 10^7	0.22 ± 0.03	3.3
p38α, GST−MK2a 1−400	(8.1 ± 1.1) × 10^7	0.08 ± 0.04	1.0

The interaction between p38α and GST−MK2a 1−400 was first examined by surface plasmon resonance. Equilibrium binding data, fit to a 1/1 binding model, demonstrated this interaction to be of high affinity; K_d = 2.5 nM for the complex (Table 1). Similar experiments conducted with carboxy-terminally truncated GST−MK2a 1−369 and GST−MK2b were unable to detect an interaction with p38α (data not shown), suggesting the importance of the putative carboxy-terminal docking domain of MK2a for high-affinity complex formation with p38α.

To elucidate the role of the carboxy-terminal docking domain of MK2a, an amino-terminal FITC-labeled peptide containing residues 370−400 was synthesized for binding studies. Stopped-flow fluorescence experiments indicated that K_d = 8.4 nM (k_{on} = 1.9 × 10^8 M^{-1} s^{-1}; k_{off} = 1.6 s^{-1}) for the p38α·FITC−MK2a 370−400 complex (Table 2 and Figure 1). To confirm that the FITC label was not contributing to the binding affinity of the peptide, a second peptide lacking the FITC label was also prepared for study. Solution ligand-exchange competition stopped-flow experiments between the two peptides show that FITC has minimal influence on the interaction (Table 2). These data imply that the interaction between p38α and MK2a is primarily mediated through the last 30 carboxy-terminal amino acid residues of MK2a.

The FITC-labeled MK2a peptide was employed as a probe in ligand-exchange competition experiments to determine the solution binding kinetics of GST−MK2a 1−400 and p38α. The association (k_{on} = 8.1 × 10^7 M^{-1} s^{-1}) and dissociation (k_{off} = 0.08 s^{-1}) rate constants of binding were determined by stopped-flow fluorescence to yield a K_d of 1.0 nM (Table 2). The equilibrium dissociation constant for the p38α·GST−MK2a 1−400 complex determined by stopped-flow fluorescence experiments is consistent with the value determined by SPR experiments.

Ligand-exchange stopped-flow fluorescence competition kinetic experiments were also performed with a construct of MK2a lacking the first 50 amino-terminal residues. Solution stopped-flow experiments yielded a K_d of 3.3 nM (k_{on} = 6.6 × 10^7 M^{-1} s^{-1}; k_{off} = 0.22 s^{-1}) for the p38α·6His−MK2a 51−400 complex (Table 2). These data are in good agreement with the SPR data obtained with full-length

Table 3: Isothermal Titration Calorimetry Analysis of p38α·MK2a Complexes

cell sample	titrant	K_d (nM)	[NaCl] (M)	ΔH (kcal/mol)	$T\Delta S$ (kcal/mol)	N
GST−MK2a 1−400	p38α	≤10	0.2	−17.3 ± 1.2[a]	≥−6.4	0.7 ± 0.1[a]
GST−MK2a 1−400	p38α	106	0.4	−11.0 ± 0.1[b]	≥−1.5	0.9
MK2a 1−400	p38α	≤10	0.2	−16.1 ± 0.1[b]	≥−5.2	0.8
6His−MK2a 51−400	p38α	≤10	0.2	−20.1 ± 0.4[a]	≥−9.0	0.8 ± 0.1[a]
MK2a 370−400	p38α	≤10	0.2	−9.9 ± 0.4[a]	≥−1.0	0.8 ± 0.4[a]

[a] Standard errors are calculated from data collected in multiple experiments. [b] Standard errors are calculated as the fit error from a single data set.

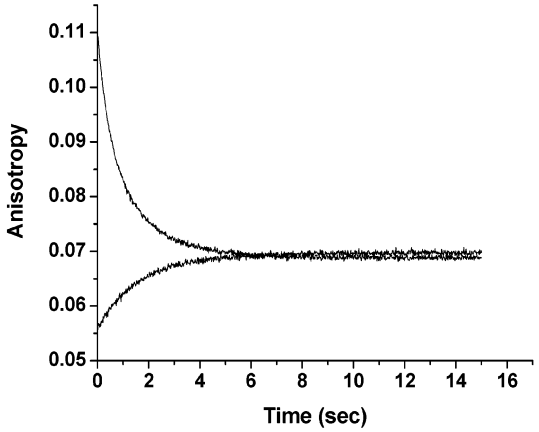

FIGURE 1: Stopped-flow fluorescence kinetic analysis of the p38α·6His−MK2a 51−400 binding interaction. Association and dissociation of 6His−MK2a 51−400 and p38α were monitored with a stopped-flow instrument in an anisotropy-based format employing a paired ligand-exchange assay. In the top curve, the dissociation of the FITC−MK2a 370−400 peptide (300 nM) from p38α (300 nM) was initiated by the addition of 6His−MK2a 51−400 (400 nM), and a new equilibrium was then reached between all three reactants. In the reverse reaction (bottom curve), dissociation of 6His−MK2a 51−400 (400 nM) from p38α (300 nM) was initiated by the addition of the FITC−MK2a 370−400 peptide (300 nM), and a new equilibrium among all three components was then reached. Both data sets were analyzed simultaneously, and nonlinear regression analysis converged to produce the solution (solid lines) yielding the following: $k_{on} = (6.6 \pm 1.9) \times 10^7$ M^{-1} s^{-1} and $k_{off} = 0.22 \pm 0.03$ s^{-1} (*38*).

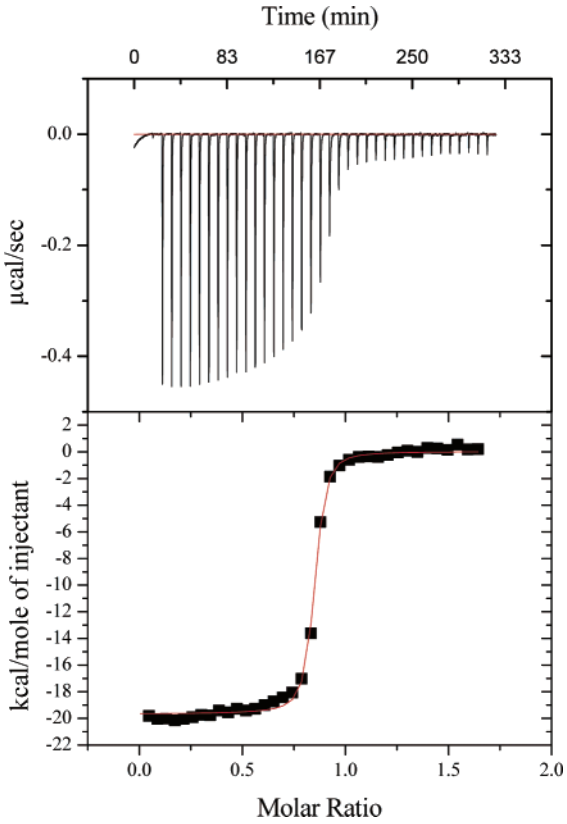

FIGURE 2: Calorimetric titration of p38α into a sample cell containing 6His−MK2a 51−400. The titration was performed at 25 °C in 20 mM TES (pH 7.0), 200 mM NaCl, and 1 mM TCEP as described in Experimental Procedures. The data were fit with a one-site binding model to obtain an N of 0.9 and a ΔH of −20.4 kcal/mol.

MK2a, indicating that the first 50 amino-terminal residues are not required for the interaction between MK2a and p38α. Experiments comparing the binding of full-length protein and peptide MK2a constructs to p38α demonstrated faster association and dissociation binding kinetics with the significantly smaller peptide constructs (data not shown). This data trend suggests that additional binding interactions may occur between full-length MK2a and p38α that are absent in the p38α·MK2a 370−400 interaction.

Isothermal titration calorimetry was used to determine the thermodynamic nature of the interaction between MK2a and p38α. The data in Table 3 show that MK2a can form a tight 1/1 complex with p38α. Due to the steepness of the titration curve shown in Figure 2, equilibrium dissociation constants could not be accurately fit to the data; however, the results suggest that the equilibrium dissociation constant for the p38α·MK2a complex is less than 10 nM. This is consistent with the stopped-flow fluorescence and SPR results.

As shown with the SPR and stopped-flow fluorescence data, 6His−MK2a 51−400 and GST−MK2a 1−400 bind to p38α with similar affinities. The origin of the 2−3 kcal/mol difference in enthalpy between these two constructs is not clear at this time; however, it appears to be linked to the first 50 amino-terminal residues of MK2a. Upon removal of the GST tag from GST−MK2a 1−400 by TEV cleavage, MK2a 1−400 was found to bind to p38α with an affinity and an enthalpy similar to those of GST−MK2a 1−400, confirming that the GST tag was not interfering with the interaction.

The interaction between MK2a and p38α was observed to be enthalpically driven. Increasing the ionic strength of the buffer resulted in a reduction in binding affinity, as observed by both SPR (Table 1) and ITC (Table 3). This finding supports a model in which electrostatic interactions between the Lys/Arg-rich carboxy terminus of MK2a and two acidic regions on p38α contribute significantly to the interactions between MK2a and p38α. Additional evidence in support of this model is the observation that the interaction between MK2a 370−400 and p38α is primarily enthalpic.

SPR experiments were conducted to study whether phosphorylation affects the interaction between p38α and MK2a. Activated p38α was found to bind GST−MK2a 1−400 with an affinity similar to that of nonactivated p38α; $K_d = 6.3$

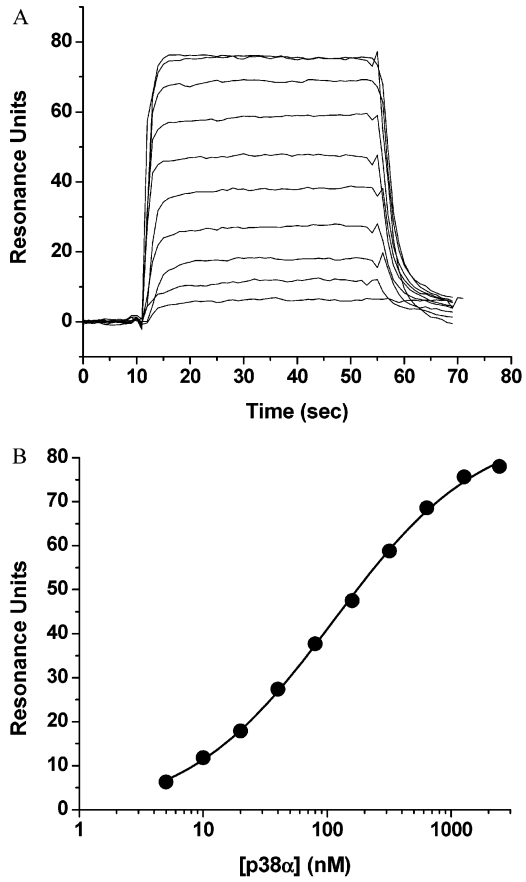

FIGURE 3: Equilibrium dissociation constant for the p38α·activated MK2a complex. (A) Sensorgrams depicting the binding of p38α at various concentrations to immobilized GST-activated MK2a 1−400 at a flow rate of 30 μL/min and 25 °C. Sensorgrams represent control flow cell-subtracted data. (B) The K_d for the p38α·MK2a interaction was obtained by applying a single-site binding model to equilibrium data obtained from the above concentration series. The equilibrium dissociation constant was determined by regression analysis (K_d = 104 ± 30 nM).

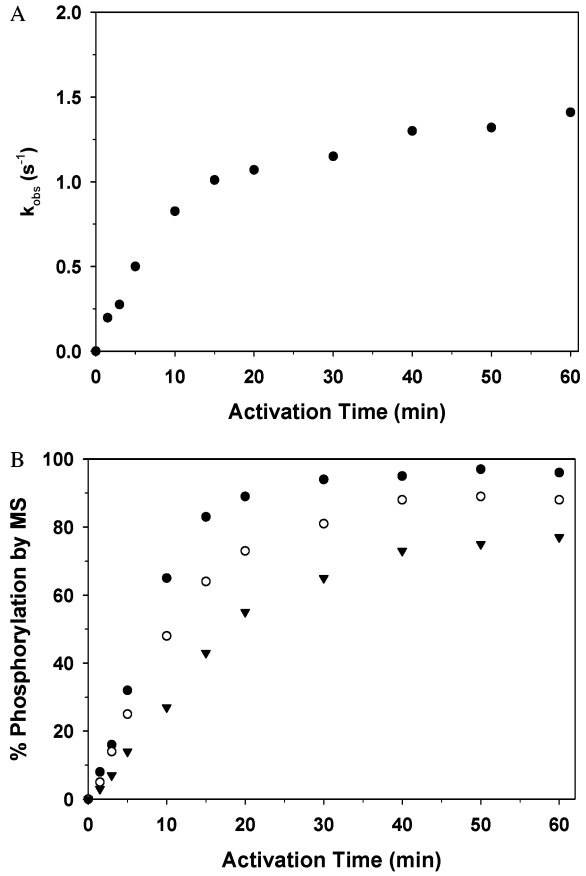

FIGURE 4: Activation of 6His−MK2a 51−400 by p38α. (A) 6His−MK2a 51−400 (11.5 μM) was phosphorylated by 95 nM activated p38α in the presence of 1 mM ATP. The reactions were quenched at various times (activation time) with 100 mM EDTA. The observed rate constants, k_{obs}, of activated 6His−MK2a 51−400 (1 nM) catalysis of GST−LSP1 179−339 (10 μM) phosphorylation were measured in the presence of 100 μM [γ-^{33}P]ATP (800 Ci/mol) as described in Experimental Procedures. (B) An aliquot of phosphorylated 6His−MK2a 51−400 at each activation time in panel A was digested with trypsin. Three peptides were observed to be phosphorylated by MS analysis: residues 213−242, containing T222 (●); residues 243−276, containing S272 (○); and residues 331−340, containing T334 (▼). The extent of phosphorylation as a function of activation time was plotted for each peptide.

nM for the activated p38α·MK2a complex, and K_d = 2.5 nM for the nonactivated p38α·MK2a complex (Table 1). A significant reduction in binding affinity occurs once MK2a is activated by active p38α; the K_d for the p38α·activated MK2a complex was observed to be 104 nM (Table 1 and Figure 3). A similar affinity was observed between activated p38α and activated MK2a (K_d = 60 nM). These results are consistent with the premise that enzyme binds product with less affinity than substrate. The mechanism by which phosphorylation attenuates affinity is currently unknown.

Steady-State Kinetic Analysis of p38α·MK2a Complex Catalysis and Function. Signal transduction studies of the p38 pathway, including immunocomplex kinase assays, pull-down experiments, and non-steady-state kinetics, indicate that p38α and p38*β* phosphorylate two splice variants of MK2 (*25*−*32*). Splice variant MK2a has, indeed, been observed to form tight (1−10 nM) complexes with p38α by SPR, stopped-flow fluorescence, and ITC. Catalysis of MK2a and MK2b splice variant phosphorylation by activated p38α was assessed under steady-state conditions to determine the maximal rates, k_{cat}, of signal transduction through the signaling complexes. In addition, the specificity constant, k_{cat}/K_M, which governs the rate of signal transduction through the signaling complexes at low substrate concentrations, was measured.

Steady-state kinetic experiments involving kinases, such as p38α, are often complicated by the phosphorylation of the substrate at more than one position. The enzyme has been observed previously to phosphorylate MK2a at more than one residue: T25, T222, S272, and T334 (*33*). After activation of 6His−MK2a 51−400 by activated p38α, tryptic digestion and mass spectrometry analysis were utilized to identify three phosphopeptides containing residues T222, S272, and T334. These peptides were observed to be phosphorylated at similar but distinct rates (Figure 4). True Michaelis−Menten constants describing MK2 phosphorylation by activated p38α could not be obtained, because multiple products were formed at distinct rates. Instead, apparent catalytic rate constants (k_{cat}^{app}) and apparent Michaelis constants (K_M^{app}) that approximated the true constants were obtained in the steady-state kinetic studies.

Activated p38α was observed to be an efficient catalyst of MK2a splice variant phosphorylation and activation (Table

Table 4: Steady-State Kinetic Analysis of p38α Phosphorylation of MK2[a]

constant substrate	varied substrate	K_M^{app} (μM)	k_{cat}^{app} (s^{-1})	k_{cat}^{app}/K_M^{app} (M^{-1} s^{-1})
ATP[b]	6His−MK2a 51−400	0.043 ± 0.012	0.049 ± 0.002	1.1×10^6
6His−MK2a 51−400[c]	ATP	24.9 ± 2.7	0.099 ± 0.003	4.0×10^3
ATP[b]	6His−MK2a 51−369	>5	>0.002	NA
ATP[b]	GST−MK2a 1−400	0.108 ± 0.013	0.33 ± 0.01	3.1×10^6
ATP[b]	GST−MK2b 41−370	>5	>0.009	NA

[a] The maximum rates of activated p38α (1 nM) catalysis, k_{cat}^{app}, and the concentrations of varied substrates required for half-maximal activity, K_M^{app}, were determined by fitting plots of initial velocity vs substrate concentration to the Michaelis−Menten equation. [b] The ATP concentration was 150 μM. [c] The 6His−MK2a 51−400 concentration was 1.5 μM.

4). The apparent catalytic rate constant ($k_{cat}^{app} = 0.05$ s^{-1}) and the apparent Michaelis constant ($K_M^{app} = 43$ nM) governing the phosphorylation and activation of 6His−MK2a 51−400 indicate that the p38α·MK2a signaling complex is the most proficient p38 pathway signaling complex yet to be discovered. The apparent second-order rate constant of catalysis ($k_{cat}^{app}/K_M^{app} = 1.1 \times 10^6$ M^{-1} s^{-1}) indicates that p38α is an efficient activator of MK2a under conditions where the substrate is not present at saturating concentrations, as is often the case in the context of the cell (Table 4). p38α was also an efficient catalyst of GST−MK2a 1−400 (Figure 5) and MK2a 1−400 phosphorylation (data not shown). The concentration of MK2a required for half-maximal catalysis (K_M^{app}) does not represent the true affinity of the activated p38α·MK2a complex; the affinity of the complex was determined to be 1 order of magnitude tighter by SPR ($K_d = 6$ nM for the activated p38α·MK2a complex). This difference between the observed K_d and K_M^{app} values is not unexpected, because the enzyme, substrate, and enzyme·substrate complex are not in rapid equilibrium ($k_{cat}^{app} \approx k_{off}$), and the kinetic constants are apparent or average constants. Nevertheless, the kinetic data are consistent with the biophysical data in indicating that activated p38α and MK2a form a tight, functional signaling complex.

The time-dependent activation of MK2a by p38α was assessed by the observed rates of MK2a catalysis of GST−LSP1 179−339 phosphorylation (Figure 4). Maximal activation of the 6His−MK2a 51−400 kinase ($k_{obs} = 1.3$ s^{-1}) appears to coincide with the phosphorylation of three residues: T222, S272, and T334. Residue T334, which becomes phosphorylated prior to nuclear export (*34*), was phosphorylated at a slower rate than the first two residues located within the kinase domain. The initial rate of T334 phosphorylation was approximately 2−3 times slower than the rates of T222 and S272 phosphorylation.

To measure the contribution of the MK2a carboxy-terminal docking domain to catalysis and function of the p38α·MK2a signaling complex, steady-state phosphorylation of two MK2 substrates lacking the docking domain, 6His−MK2a 51−369 and GST−MK2b, was carried out. In agreement with previous signal transduction studies (*27*, *29*, *30*), and our biophysical analyses of the complexes, removal of the carboxy-terminal docking domain of MK2a resulted in a significant decrease in binding affinity for p38α (Table 4). The K_M^{app} for the 6His−MK2a 51−369 substrate lacking the p38α docking domain was greater than 5 μM. This suggests that the interaction between the Lys/Arg-rich carboxy-terminal tail of MK2a and p38α provides essential binding energy for meeting signaling requirements when constituents of the p38 pathway are not necessarily abundant. In comparing the steady-state kinetic parameters describing

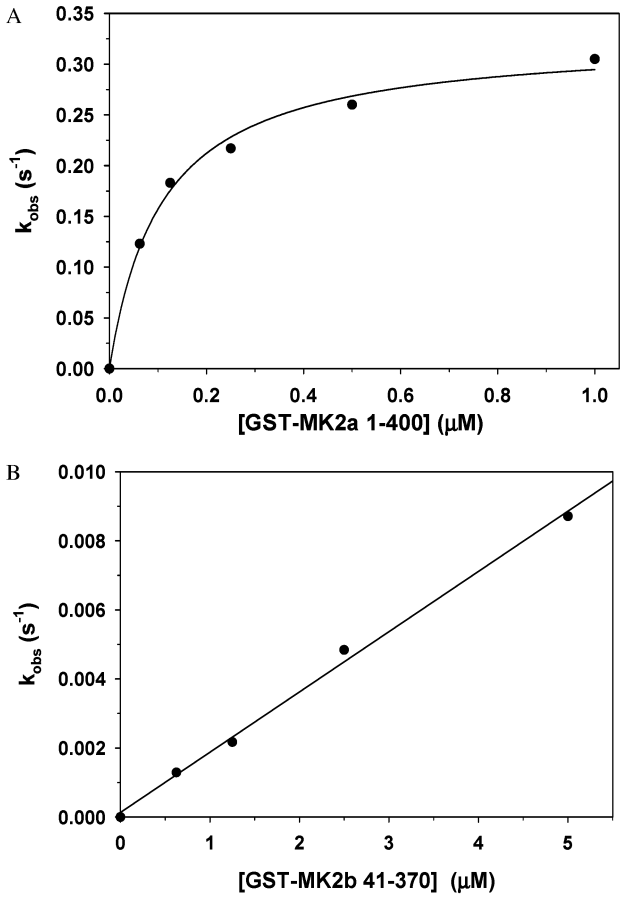

FIGURE 5: Steady-state phosphorylation of MK2a and MK2b by p38α. (A) GST−MK2a 1−400 was phosphorylated by activated p38α (1 nM) in the presence of 150 μM [γ-^{33}P]ATP (2000 Ci/mol). The maximum rate of phosphorylation ($k_{cat}^{app} = 0.33 \pm 0.01$ s^{-1}) and the Michaelis constant ($K_M^{app} = 108 \pm 13$ nM) were obtained from hyperbolic curve fits to the Michaelis−Menten equation. (B) GST−MK2b 41−370 was phosphorylated by activated p38α (5 nM) in the presence of 150 μM [γ-^{33}P]ATP (2000 Ci/mol). A plot of k_{obs} vs [GST−MK2b 41−370] was fit by linear regression to indicate that the K_M^{app} for the reaction is >5 μM.

p38α phosphorylation of GST−MK2a and GST−MK2b, we found it was evident that GST−MK2b bound active p38α with a significantly lower affinity; K_M^{app} for the reaction was greater than 5 μM (Figure 5). These data suggest that in the absence of other signaling components, the concentration of MK2a required for signal transduction downstream of p38α is approximately 2 orders of magnitude less than the concentration of MK2b required for signaling (Table 4). Therefore, the 30-amino acid docking domain of MK2a (MK2a 370−400) appears to be important for signal transduction mediated by p38α.

Table 5: Inhibition of p38α by MK2a 370−400[a]

substrate	inhibitor	IC_{50} (nM)
6His−MK2a 51−400[b]	MK2a 370−400	59.9 ± 4.4
6His−MK2a 51−400[b]	FITC−MK2a 370−400	38.5 ± 1.8
GST−ATF-2 1−109[c]	MK2a 370−400	23.0 ± 3.7

[a] The concentrations of MK2a 370−400 required for half-maximal inhibition, IC_{50}, of MK2a or ATF-2 phosphorylation by activated p38α (250 pM) were determined. The experiments were performed in triplicate. [b] The level of inhibition of 6His−MK2a 51−400 (25 nM) activation was measured by the reduction in the level of 6His−MK2a 51−400-dependent phosphorylation of GST−LSP1 179−339 (10 μM). [c] The inhibition of GST−ATF-2 1−109 (10 μM) phosphorylation was assessed.

The MK2a Carboxy-Terminal Domain Is a Potent Inhibitor of p38α·MK2a Function. Steady-state kinetic and thermodynamic binding studies suggest that the carboxy-terminal domain of MK2a should be a potent inhibitor of p38α. To test this hypothesis, the inhibition of p38α catalysis of MK2a and ATF-2 phosphorylation by the MK2a 370−400 carboxy-terminal domain was studied. The MK2a 370−400 peptide and the FITC−MK2a 370−400 peptide designed for stopped-flow experiments were observed to be potent inhibitors of MK2a phosphorylation (Table 5). The data confirm a high-affinity interaction between the MK2a carboxy-terminal domain and p38α. The MK2a 370−400 domain also potently inhibited the phosphorylation of ATF-2, demonstrating that the carboxy terminus of MK2a does not specifically block MK2a activation, but prevents the phosphorylation of ATF-2 *in vitro*.

DISCUSSION

The classical approach to the study of the signal transduction pathways, involving phosphorylation, immunoprecipitation, and pull-down assays, has been based on the premise that they are simple linear cascades that transfer sequential downstream signals via the phosphorylation and activation of downstream kinases and effector proteins. Cellular and genetic deletion studies of these pathways indicate that the pathways are far more sophisticated. We have performed the first thermodynamic and steady-state kinetic analyses of p38α·MK2 signaling complexes to gain new insight into signaling function, catalysis, and inhibition. High-affinity complexes, containing both activated and nonactivated forms of p38α and MK2a, were characterized by ITC, stopped-flow fluorescence, SPR, and steady-state kinetics, in defining and quantifying signal transduction through this pathway.

The identification of high-affinity p38α·MK2a complexes, exhibiting K_d values of 1−10 nM, and p38α·MK2a 370−400 carboxy-terminal domain complexes with similar affinities indicates that MK2a residues 370−400 form a p38α docking domain. The high-affinity interaction identified between MK2a 370−400 and p38α suggests that the majority of the binding energy between MK2a and p38α is derived from the carboxy-terminal docking domain. Differences in the binding kinetics and the reduced enthalpy of binding of MK2a 370−400 versus full-length MK2a indicate that additional contacts outside of the p38α docking groove contribute only a small amount of additional binding energy, but may aid in binding specificity. These observations are consistent with data obtained from binding studies between p38α and a homologue of MK2a, MK3, in which the binding affinity between p38α and MK3 was greatly reduced upon mutation of basic residues in the carboxy terminus of MK3 (*26*). The decrease in the affinity of the p38α·MK2a complex coincident with an increase in ionic strength is also consistent with an ionic interaction between MK2a 370−400 and the acidic domains (CD and ED) of the p38α docking groove. Mutations of acidic residues in the CD and ED domains of p38α resulted in significant reductions in the affinity of p38α for MK3 (*26*). Thus, ionic interactions between MK2a and the CD and ED domains of the p38α docking groove are likely contributing to the strong affinity of the complex.

Hydrophobic interactions between numerous hydrophobic residues of MK2a 370−400 and the docking groove of p38α could also contribute significant binding energy to the complex. X-ray crystallographic and mutagenesis studies of p38α·MKK3b peptide and p38α·MEF2A peptide complexes indicate that hydrophobic interactions are critical for the formation of these complexes (*39*). Thus, in addition to ionic interactions, hydrophobic interactions may also make substantial contributions to the affinity of the p38α·MK2a complex.

The interaction between the MK2a docking domain and p38α is not essential for MK2 phosphorylation and activation, but it appears to be required for efficient activation of MK2a under conditions where substrate MK2a concentrations are low, as might be expected in a cellular context. The catalytic efficiency of MK2b phosphorylation by p38α, as measured by the specificity constant, is at least 2 orders of magnitude lower than the catalytic efficiency of MK2a phosphorylation, $1.1 \times 10^6\ M^{-1}\ s^{-1}$. This is consistent with the observation that the mutations of key MK2a docking domain residues (385−388) result in a significant reduction in the level of activation of MK2a by p38 in cells (*23*), and it is consistent with the observation that the production of TNFα from macrophages expressing full-length MK2a is significantly greater than the production of TNFα in the presence of MK2b and MK2 constructs lacking the docking domain that is required for efficient activation of MK2 by p38α (*2*).

While the complex formed between MK2a and p38α is tight, it must possess flexibility to allow for the phosphorylation of three spatially distinct residues. The steady-state kinetic studies of MK2a phosphorylation have demonstrated that residues in the MK2a kinase domain (T222 and S272) and a residue outside the kinase domain (T334) are phosphorylated at similar but distinct rates by p38α. Phosphorylation of these three residues has been shown in mutagenesis studies to be required for maximal activation of MK2a *in vitro* and in cells (*33*). The SPR binding studies also indicate that p38α retains substantial affinity for activated MK2a that is phosphorylated at each of the three residues. The binding affinity of activated p38α for fully phosphorylated MK2a was only 1 order of magnitude lower than the affinity of activated p38α for nonactivated MK2a. Thus, the data suggest that the docking of MK2a into the docking groove of p38α allows for the phosphorylation of the three MK2a residues required for activation, and that substantial docking affinity is maintained during the phosphorylation of these residues.

The observation that MK2a residue T334 is phosphorylated by p38α at a rate that is 2−3 times slower than that of residues T222 and S272 could be significant in allowing for the phosphorylation of nuclear MK2a substrates prior to nuclear export, if the relative rates of phosphorylation are similar in the cell. MK2 is believed to phosphorylate serum response factor, E47, and ER81 in the nucleus (*40*). The kinetics of MK2a activation suggest that MK2a can be partially activated by the phosphorylation of residues T222 and S272 prior to complete phosphorylation of residue T334. These data are supported by cellular mutagenesis experiments demonstrating that the level of activation of a T334A mutant of MK2a in COS cells stimulated with arsenite is 80% of the level of wild-type MK2a activation (*33*). If the kinetics of MK2a phosphorylation are similar in the context of the cell, then activated MK2a enzymes have a limited amount of time to phosphorylate nuclear substrates prior to the exposure of the nuclear export signal upon phosphorylation of residue T334 (*23*, *24*, *34*).

In the cytoplasm, activated MK2a modulates the activities of HSP27, a lymphocyte motility protein, LSP1 (*34*), and AU-rich element binding proteins, including tristetraprolin (*19*−*22*). MK2 is believed to modulate inflammatory cytokine message stability and translation through the phosphorylation of transactivating factors that bind to the AU-rich elements of cytokine mRNA (*22*). Therefore, the inhibition of activated MK2a is a target for blocking the production of inflammatory cytokines.

The preferred method of blocking signal transduction for therapeutic purposes has been the development of active site inhibitors of the kinases involved in these pathways. One concern with this approach is that ATP competitive inhibitors of kinases are inherently cross-reactive, due to the homology shared by kinase active sites. This makes the development of selective active site kinase inhibitors difficult. A novel approach to the development of selective kinase inhibitors is the pursuit of agents that perturb the docking interactions between kinases, and their upstream and downstream signaling partners. The peptide comprising MK2a docking domain residues 370−400 is a potent inhibitor of p38α-dependent phosphorylation of MK2a and ATF-2. The MK2a 370−400 docking domain inhibitor may also perturb the interaction between p38α and the upstream activators, such as MKK3b (*39*), to preclude activation of p38α, but this has not yet been tested. The mechanism of inhibition described validates the principle that perturbation of the docking interactions between p38 and its substrates is effective in blocking the activation of the downstream signaling partners. The development of novel inhibitors of the docking interactions between p38 and its signaling partners appears to be a reasonable approach for inhibiting this pathway; such an approach could also be applied to the inhibition of signal transduction in other kinase pathways that involve docking interactions between kinases and their signaling partners.

ACKNOWLEDGMENT

We are indebted to the following individuals for their contributions to this work: Gerry Bell and Natalie Fuschetto for assistance in the purification of protein reagents, Lore Gruenbaum for a critical reading of the manuscript, and Nicole Furlani and Achim Lietz for their technical contributions to the SPR work.

REFERENCES

1. Hannigan, M. O., Zhan, L., Ai, Y., Kotlyarov, A., Gaestel, M., and Huang, C. K. (2001) Abnormal migration phenotype of mitogen-activated protein kinase-activated protein kinase 2-/- neutrophils in Zigmond chambers containing formyl-methionyl-leucyl-phenylalanine, *J. Immunol. 167*, 3953−3961.
2. Kotlyarov, A., Yannani, Y., Fritz, S., Laass, K., Telliez, J.-B., Pitman, D., Liu, L.-L., and Gaestel, M. (2002) Distinct cellular functions of MK2, *Mol. Cell. Biol. 22*, 4827−4835.
3. Wang, X., Xu, L., Wang, H., Young, P. R., Gaestel, M., and Feurstein, G. Z. (2002) Mitogen-activated protein kinase-activated protein (MAPKAP) kinase 2 deficiency protects brain from ischemic injury in mice, *J. Biol. Chem. 277*, 43968−43972.
4. Kontoyiannis, D., Boulougouris, G., Manoloukos, M., Armaka, M., Apostoloki, M., Pizarro, T., Kotlyarov, A., Forster, I., Flavell, R., Gaestel, M., Tsichlis, P., Cominelli, F., and Kollias, G. (2002) Genetic dissection of the cellular pathways and signaling mechanisms in modeled tumor necrosis factor-induced Crohn's-like inflammatory bowel disease, *J. Exp. Med. 196*, 1563−1574.
5. Lee, J. C., Kassis, S., Kumar, S., Badger, A., and Adams, J. L (1999) p38 mitogen-activated protein kinase inhibitor: mechanisms and therapeutic potentials, *Pharmacol. Ther. 82*, 389−397.
6. Allen, M., Svensson, L., Roach, M., Hambor, J., McNeish, J., and Gabel, C. A. (2000) Deficiency of the stress kinase p38α results in embryonic lethality: characterization of the kinase dependence of stress responses of enzyme-deficient embryonic stem cells, *J. Exp. Med. 191*, 859−870.
7. Lee, J. C., Badger, A. M., Griswold, D. E., Dunnington, D., Truneh, A., Votta, B., White, J. R., Young, P. R., and Bender, P. E. (1993) Bicyclic imidazoles as a novel class of cytokine biosynthesis inhibitors, *Ann. N.Y. Acad. Sci. 696*, 149−170.
8. Pargellis, C., Tong, L., Churchill, L., Cirillo, P. F., Gilmore, T., Graham, A. G., Grob, P. M., Hickey, E. R., Moss, N., Pav, S., and Regan, J. (2002) Inhibition of p38 MAP kinase by utilizing a novel allosteric binding site, *Nat. Struct. Biol. 9*, 268−272.
9. Pargellis, C., and Regan, J. R. (2003) Inhibitors of p38 mitogen-activated protein kinase for the treatment of rheumatoid arthritis, *Curr. Opin. Invest. Drugs 4*, 566−571.
10. Dinarello, C. A. (1991) Inflammatory cytokines: interleukin-1 and tumor necrosis factor as effector molecules in autoimmune diseases, *Curr. Opin. Immunol. 3*, 941−948.
11. Feldmann, M., Brennan, F. M., and Maini, R. N. (1996) Role of cytokines in rheumatoid arthritis, *Annu. Rev. Immunol. 14*, 397−440.
12. Rankin, E. C., Choy, E. H., Kassimos, D., Kingsley, G. H., Sopwith, A. M., Isenberg, D. A., and Panayi, G. S. (1995) The therapeutic effects of an engineered human anti-tumour necrosis factor alpha antibody (CDP571) in rheumatoid arthritis, *Br. J. Rheumatol. 34*, 334−342.
13. Nuki, K. G., Bresnihan, B., Bear, M. B., and McCabe, D. (2002) Long-term safety and maintenance of clinical improvement following treatment with anakinra (recombinant human interleukin-1 receptor antagonist) in patients with rheumatoid arthritis: extension phase of a randomized, double-blind, placibo-controlled trial, *Arthritis Rheum. 46*, 2838−2846.
14. Stokoe, D., Campbell, D. G., Nakielny, S., Hidaka, H., Leevers, S. J., Marshall, C., and Cohen, P. (1992) MAPKAP kinase-2; a novel protein kinase activated by mitogen-activated protein kinase, *EMBO J. 11*, 3985−3994.
15. Stokoe, D., Caudwell, F. B., Cohen, P. T. W., and Cohen, P. (1993) The substrate specificity and structure of mitogen-activated protein (MAP) kinase-activated protein kinase-2, *Biochem. J. 296*, 843−849.
16. Freshney, N. W., Rawlinson, L., Guesdon, F., Jones, E., Cowley, S., Hsuan, J., and Saklatvala, J. (1994) Interleukin-1 activates a novel protein kinase cascade that results in the phosphorylation of Hsp27, *Cell 78*, 1039−1049.
17. Rouse, J., Cohen, P., Trigon, S., Morange, M., Alonso-Llamazares, A., Zamanillo, D., Hunt, T., and Nebreda, A. R. (1994) A novel kinase cascade triggered by stress and heat shock that stimulates MAPKAP kinase-2 and phosphorylation of the small heat shock protein, *Cell 78*, 1027−1037.
18. Cuenda, A., Rouse, J., Doza, Y. N., Meier, R., Cohen, P., Gallagher, T. F., Young, P. R., and Lee, J. C. (1995) SB 203580

is a specific inhibitor of a MAP kinase homologue which is stimulated by cellular stresses and interleukin-1, *FEBS Lett. 364*, 229−233.
19. Kotlyarov, A., Neininger, A., Schubert, C., Eckert, R., Birchmeier, C., Volk, H. D., and Gaestel, M. (1999) MAPKAP kinase 2 is essential for LPS-induced TNF-α biosynthesis, *Nat. Cell Biol. 1*, 94−97.
20. Neiniger, A., Kontoyiannis, D., Kotlyarov, A., Winzen, R., Eckert, R., Volk, H. D., Holtmann, H., Kollias, G., and Gaestel, M. (2002) MK2 targets AU-rich elements and regulates biosythesis of tumor necrosis factor and interleukin-6 independently at different post-transcriptional levels, *J. Biol. Chem. 277*, 3065−3068.
21. Mahtani, K. R., Brook, M., Dean, J. L., Sully, G., Saklatvala, J., and Clark, A. R. (2001) Mitogen-activated protein kinase p38 controls the expression and posttranslational modification of tristetraprolin, a regulator of tumor necrosis factor alpha mRNA stability, *Mol. Cell. Biol. 21*, 6461−6469.
22. Stoecklin, G., Stubbs, T., Kedersha, N., Wax, S., Rigby, W. F. C., Blackwell, T. K., and Anderson, P. (2004) MK2-induced tristetraprolin: 14-3-3 complexes prevent stress granule association and ARE-mRNA decay, *EMBO J. 23*, 1313−1324.
23. Ben-Levy, R., Hooper, S., Wilson, R., Peterson, H. F., and Marshall, C. J. (1998) Nuclear export of the stress-activated protein kinase p38 mediated by its substrate MAPKAP kinase-2, *Curr. Biol. 8*, 1049−1057.
24. Engel, K., Kotlyarov, A., and Gaestel, M. (1998) Leptomycin B-sensitive nuclear export of MAPKAP kinase 2 is regulated by phosphorylation, *EMBO J. 17*, 3363−3371.
25. Tanoue, T., Adachi, M., Moriguchi, T., and Nishida, E. (2000) A conserved docking motif in MAP kinases common to substrates, activators and regulators, *Nat. Cell Biol. 2*, 110−116.
26. Tanoue, T., Maeda, R., Adachi, M., and Nishida, E. (2001) Identification of a docking groove on ERK and p38 MAP kinases that regulates the specificity of docking interactions, *EMBO J. 20*, 466−479.
27. Smith, J. A., Poteet-Smith, C. E., Lannigan, D. A., Freed, T. A., Zoltoski, A. J., and Sturgill, T. W. (2000) Creation of a stress-activated p90 ribosomal S6 kinase. The carboxyl-terminal tail of the MAPK-activated protein kinases dictates the signal transduction pathway in which they function, *J. Biol. Chem. 275*, 31588−31593.
28. Hawkins, J., Zheng, S., Frantz, B., and LoGrasso, P. (2000) p38 map kinase substrate specificity differs greatly for protein and peptide substrates, *Arch. Biochem. Biophys. 382*, 310−313.
29. Kumar, S., McDonnell, P. C., Gum, R. J., Hand, A. T., Lee, J. C., and Young, P. R. (1997) Novel homologues of CSB/p38 MAP kinase: activation, substrate specificity and sensitivity to inhibtion by pyridinyl imidazoles, *Biochem. Biophys. Res. Commun. 235*, 533−538.
30. Gum, R. J., and Young, P. R. (1999) Identification of two distinct regions of p38 MAPK required for substrate binding and phosphorylation, *Biochem. Biophys. Res. Commun. 266*, 284−289.
31. Zu, Y.-L., Wu, F., Gilchrist, A., Ai, Y., Labadia, M. E., and Huang, C.-K. (1994) The primary structure of a human MAP kinase activated protein kinase 2, *Biochem. Biophys. Res. Commun. 200*, 1118−1124.
32. Zu, Y.-L., Ai, Y., and Huang, C.-K. (1995) Characterization of an autoinhibitory domain in human mitogen-activated protein kinase-activated protein kinase 2, *J. Biol. Chem. 270*, 202−206.
33. Ben-Levy, R., Leighton, I. A., Doza, Y. N., Attwood, P., Morrice, N., Marshall, C. J., and Cohen, P. (1995) Identification of novel phosphorylation sites required for activation of MAPKAP kinase-2, *EMBO J. 14*, 5920−5930.
34. Neineinger, A., Theilemann, H., and Gaestel, M. (2001) FRET-based detection of different conformations of MK2, *EMBO Rep. 21*, 703−708.
35. Kroe, R. R., Regan, J., Proto, A., Peet, G. W., Roy, T., Landro, L. D., Fuschetto, N. G., Pargellis, C. A., and Ingraham, R. H. (2003) Thermal denaturation: a method to rank slow binding, high-affinity p38α MAP kinase inhibitors, *J. Med. Chem. 46*, 4669−4675.
36. Johnsson, B., Löfås, S., and Lindquist, G. (1991) Immobilization of proteins to a carboxymethyldextran-modified gold surface for biospecific interaction analysis in surface plasmon resonance sensors, *Anal. Biochem. 198*, 268−277.
37. Morelock, M. M., Ingraham, R. H., Betageri, R., and Jakes, S. (1995) Determination of receptor−ligand kinetic and equilibrium binding constants using surface plasmon resonance: application to the Lck SH2 domain and phosphotyrosyl peptides, *J. Med. Chem. 38*, 1309−1318.
38. Morelock, M. M., Pargellis, C. A., Graham, E. T., Lamarre, D., and Jung, G. (1995) Time-resolved ligand exchange reactions: kinetic models for competitive inhibitors with recombinant human renin, *J. Med. Chem. 38*, 1751−1761.
39. Chang, C.-I., Xu, B.-E., Akella, R., Cobb, M. H., and Goldsmith, E. J. (2002) Crystal structures of MAP kinase p38 complexed to the docking sites on its nuclear substrate MEF2A and activator MKK3b, *Mol. Cell 9*, 1241−1249.
40. Shi, Y., and Gaestel, M. (2002) In the cellular garden of forking paths: how p38 MAPKs signal for downstream assistance, *Biol. Chem. 383*, 1519−1536.

BI049508V